Properties of Metal–Metal Single Bonds. Vibrational and Electronic Spectra of Binuclear Rhodium(II) and Iridium(II) Isocyanide Complexes with Comparisons to Mn₂(CO)₁₀

Vincent M. Miskowski,*[1a] Terrance P. Smith,[1a] Thomas M. Loehr,[1b] and Harry B. Gray*[1a]

Contribution No. 7183 from the Arthur Amos Noyes Laboratory, California Institute of Technology, Pasadena, California 91125, and the Oregon Graduate Center, Beaverton, Oregon 96006. Received May 2, 1985

Abstract: Vibrational and electronic spectra of $Rh_2b_4L_2^{n+}$, $Rh_2(TMB)_4L_2^{n+}$ (b = 1,3-diisocyanopropane; TMB = 2,5-dimethyl-2,5-diisocyanohexane; L = H_2O, CH_3CN ($n = 4$); L = Cl, Br, I, N_3, NCS ($n = 2$)), and $Ir_2(TMB)_4L_2^{2+}$ (L = Cl, Br, I) have been measured. The three stretching vibrations of the linear M_2L_2 core are assigned and the M_2 force constants are shown to be ~ 0.9–1.6 mdyn/Å. The electronic spectra are dominated by an intense (oscillator strength 0.6–1.0) $d\sigma \rightarrow d\sigma^*$ transition. Variation in the maximum of this band over the range 33 000 to 24 000 cm⁻¹ (Rh_2^{4+}) or 37 000 to 30 000 cm⁻¹ (Ir_2^{4+}) as a function of the axial ligand is attributed to mixing with an $L \rightarrow d\sigma^*$ charge transfer transition. The temperature dependences of the $d\sigma \rightarrow d\sigma^*$ transitions of the Rh_2^{4+} complexes and $Mn_2(CO)_{10}$ have been analyzed by the method of moments and shown to be consistent with a large excited state distortion along the metal–metal stretching coordinate. A weaker absorption near 24 000 cm⁻¹ is shown from low temperature single crystal polarized spectra of $[Rh_2(TMB)_4Cl_2](PF_6)_2$ to contain the $d\pi^* \rightarrow d\sigma^*$ and $d\delta^* \rightarrow d\sigma^*$ excitations. Other weak bands of the Rh^{II} complexes near 33 000 and 43 000 cm⁻¹ are tentatively assigned to $d\pi^*,d\delta^* \rightarrow d\sigma^*$ and $d\pi^* \rightarrow d_{x^2-y^2}$ transitions, respectively. The photochemistry of the binuclear Rh^{II} complexes is shown to be consistent with halogen radical release from the halide complexes. The excited state lifetime is less than 20 ps.

The preparation of the bridged binuclear Rh^I complex $Rh_2b_4^{2+}$ (b = 1,3-diisocyanopropane) and some of its extensive redox chemistry were reported several years ago.[2] Stimulated by the discovery[2b] of solar photochemical H_2 production in this system, we have continued[3,4] systematic investigations of the reaction chemistry of $Rh_2b_4^{n+}$ ($n = 2$, 3, 4) and of Rh and Ir analogues containing other bridging isocyanides.

Detailed spectroscopic studies give insight into the electronic structure of these units and have previously been reported for the Rh^I complexes.[5] We associate[6–9] the large decrease in rhodium–rhodium bond length upon 2-electron oxidation of the Rh^I compounds (Table I) with the existence of a single metal–metal bond in binuclear Rh^{II}, analogous to the bond in[10,11] $Mn_2(CO)_{10}$. Spectroscopic results that bear on this point will be presented in this paper for both Rh^{II} and Ir^{II} species.

Knowledge of the electronic structures of binuclear Rh^{II} and Ir^{II} is needed in order to understand the properties of the mix-

Table I. Selected Bond Lengths (Å) for Binuclear Isocyanide Complexes

complex	ref	d(M–M)	d(M–C)$_{av}$	d(M–X)
$Rh_2b_4Cl_2^{2+}$	6	2.837	1.99	2.447
$Rh_2(TMB)_4Cl_2^{2+}$	7[a]	2.770	1.98	2.43
$Rh_2(p\text{-}CNC_6H_4CH_3)_8I_2^{2+}$	8	2.785	1.98	2.735
$Ir_2(TMB)_4I_2^{2+}$	9	2.803	1.97	2.726
$Rh_2b_4^{2+}$	3d	3.243	1.96	
$Rh_2(TMB)_4^{2+}$	3d	3.262	1.95	

^{a} TMB = 2,5-dimethyl-2,5-diisocyanohexane.

ed-oxidation-state oligomers[4,12] $[Rh_2b_4]_n^{(2n+2)+}$ and of "platinum blue" species.[13] Of course, the Rh^{II} and Ir^{II} species are of interest in their own right, and the availability of data for complexes with a wide range of axial ligands has allowed us to assess the effects of this important perturbation[14] on metal–metal bonding. The high metal-ion charge causes metal-to-ligand charge-transfer transitions, which appear in the same spectroscopic region as metal–metal transitions for neutral carbonyls such as[11] $Mn_2(CO)_{10}$, to be strongly shifted to higher energy, thereby simplifying interpretation problems. These complexes also provide an interesting comparison to $Rh_2(O_2CCH_3)_4$, which has a relatively short metal–metal single bond (2.3855 Å in the dihydrate[15]) and whose electronic structure has been extensively studied.[16,17]

Experimental Section

Preparation of Compounds. The Rh^I compounds were prepared as described elsewhere.[3a,d]

$[Rh_2b_4Cl_2]\cdot6H_2O$ was prepared by bubbling Cl_2 through a stirred suspension/solution of $[Rh_2b_4]Cl_2$ in hot 6 N HCl until a homogeneous yellow solution was obtained. After the mixture was purged with N_2 to remove Cl_2 and filtered, cooling in a refrigerator overnight gave a yellow

(1) (a) California Institute of Technology. (b) Oregon Graduate Center.

(2) (a) Lewis, N. S.; Mann, K. R.; Gordon, J. G., II; Gray, H. B. *J. Am. Chem. Soc.* **1976**, *98*, 7461. (b) Mann, K. R.; Lewis, N. S.; Miskowski, V. M.; Erwin, D. K.; Hammond, G. S.; Gray, H. B. *J. Am. Chem. Soc.* **1977**, *99*, 5525.

(3) (a) Miskowski, V. M.; Nobinger, G. L.; Kliger, D. S.; Hammond, G. S.; Lewis, N. S.; Mann, K. R.; Gray, H. B. *J. Am. Chem. Soc.* **1978**, *100*, 485. (b) Mann, K. R.; Gray, H. B. *Adv. Chem. Ser.* **1979**, *No. 173*, 225. (c) Milder, S. J.; Goldbeck, R. A.; Kliger, D. S.; Gray, H. B. *J. Am. Chem. Soc.* **1980**, *102*, 6761. (d) Mann, K. R.; Thich, J. A.; Bell, R. A.; Coyle, C. A.; Gray, H. B. *Inorg. Chem.* **1980**, *19*, 2462.

(4) (a) Miskowski, V. M.; Sigal, I. S.; Mann, K. R.; Gray, H. B.; Milder, S. J.; Hammond, G. S.; Ryason, P. R. *J. Am. Chem. Soc.* **1979**, *101*, 4383. (b) Gray, H. B.; Miskowski, V. M.; Milder, S. J.; Smith, T. P.; Maverick, A. W.; Buhr, J. D.; Gladfelter, W. L.; Sigal, I. S.; Mann, K. R. *Fundam. Res. Homogeneous Catal.* **1979**, *3*, 819. (c) Sigal, I. S.; Mann, K. R.; Gray, H. B. *J. Am. Chem. Soc.* **1980**, *102*, 7252. (d) Sigal, I. S.; Gray, H. B. *J. Am. Chem. Soc.* **1981**, *103*, 2220.

(5) (a) Rice, S. F.; Gray, H. B. *J. Am. Chem. Soc.* **1981**, *103*, 1593. (b) Dallinger, R. F.; Miskowski, V. M.; Gray, H. B.; Woodruff, W. H. *J. Am. Chem. Soc.* **1981**, *103*, 1595. (c) Rice, S. F. Ph.D. Thesis, California Institute of Technology, 1982.

(6) Mann, K. R.; Bell, R. A.; Gray, H. B. *Inorg. Chem.* **1979**, *18*, 2671.

(7) Maverick, A. W. Ph.D. Thesis, California Institute of Technology, 1982.

(8) Olmstead, M. M.; Balch, A. L. *J. Organomet. Chem.* **1978**, *148*, C15.

(9) Smith, T. P. Ph.D. Thesis, California Institute of Technology, 1982.

(10) (a) Churchill, M. R.; Amoh, K. N.; Wasserman, H. J. *Inorg. Chem.* **1981**, *20*, 1609. (b) Martin, M.; Rees, B.; Mitschler, A. *Acta Crystallogr., Sect. B* **1982**, *B38*, 6.

(11) Levenson, R. A.; Gray, H. B. *J. Am. Chem. Soc.* **1975**, *97*, 6042.

(12) Mann, K. R.; Dipierro, M. J.; Gill, T. J. *J. Am. Chem. Soc.* **1980**, *102*, 3965.

(13) Ginsberg, A. P.; O'Halloran, T. V.; Fanwick, P. E.; Hollis, L. S.; Lippard, S. J. *J. Am. Chem. Soc.* **1984**, *106*, 5430.

(14) Cotton, F. A.; Bursten, B. E. *Inorg. Chem.* **1981**, *20*, 3042.

(15) Cotton, F. A.; DeBoer, B. G.; LaPrade, M. D.; Pipal, J. R.; Ucko, D. A. *Acta Crystallogr.* **1971**, *B27*, 1664.

(16) Miskowski, V. M.; Schaefer, W. P.; Sadeghi, B.; Santarsiero, B. D.; Gray, H. B. *Inorg. Chem.* **1984**, *23*, 1154.

(17) (a) Norman, J. G.; Kolari, H. J. *J. Am. Chem. Soc.* **1978**, *100*, 791. (b) Norman, J. G.; Renzoni, G. E.; Case, D. A. *J. Am. Chem. Soc.* **1979**, *101*, 5256. (c) Martin, D. S.; Webb, T. R.; Robbins, G. A.; Fanwick, P. E. *J. Am. Chem. Soc.* **1979**, *101*, 475.

Table II. Low-Frequency Vibrational Data (cm^{-1})[a]

species	ν_1	ν_2	ν_3	extra Raman line
Rh$_2$b$_4$Cl$_2$$^{2+}$, 8 M HCl(aq)	283	134	–	307
Rh$_2$b$_4$Cl$_2$$^{2+}$, solid chloride salt	–	–	236	–
Rh$_2$b$_4$Cl$_2$$^{2+}$, solid PF$_6$$^-$ salt	280	130	241	308
Rh$_2$b$_4$Br$_2$$^{2+}$, solid Br$^-$ salt	217	107	179	317
Rh$_2$b$_4$I$_2$$^{2+}$, solid I$_3$$^-$ salt	~190	88	158	~285
Rh$_2$b$_4$(OH$_2$)$_2$$^{4+}$, 1 N H$_2SO_4$(aq)	n.o.	176	–	n.o.
Rh$_2$(TMB)$_4$Cl$_2$$^{2+}$, 8 M HCl(aq)	288	158	–	n.o.
Rh$_2$(TMB)$_4$Cl$_2$$^{2+}$, CH$_3$CN	288	155	–	n.o.
Rh$_2$(TMB)$_4$Cl$_2$$^{2+}$, solid PF$_6$$^-$ salt	–	–	267	–
Rh$_2$(TMB)$_4$Br$_2$$^{2+}$, solid PF$_6$$^-$ salt	244	98,123	198	n.o.
Rh$_2$(TMB)$_4$Br$_2$$^{2+}$, PF$_6$$^-$, or SO$_4$$^{2-}$ salt in CH$_3$CN	~240	102,128	–	n.o.
Rh$_2$(TMB)$_4$Br$_2$$^{2+}$, solid SO$_4$$^{2-}$ salt	n.o.	104,120	–	n.o.
Rh$_2$(TMB)$_4$I$_2$$^{2+}$, solid SO$_4$$^{2-}$ salt	~185	88	n.o.	n.o.
Rh$_2$(TMB)$_4$I$_2$$^{2+}$, CH$_3$CN (BPh$_4$$^-$ salt)	n.o.	89	–	n.o.
Ir$_2$(TMB)$_4$Cl$_2$$^{2+}$, solid BPh$_4$$^-$ salt	297	140	274	n.o.
Ir$_2$(TMB)$_4$Br$_2$$^{2+}$, solid BPh$_4$$^-$ salt	217	128	196	n.o.
Ir$_2$(TMB)$_4$I$_2$$^{2+}$, solid BPh$_4$$^-$ salt	193	116	149	n.o.

[a] See text for explanation of designations. Dashed entries were not measured, while for entries labeled "n.o.", either no line was observed or there were interfering solvent or anion lines.

solid, which was recrystallized by cooling hot saturated solutions in aqueous HCl. All of our preparations were crystalline and homogeneous under microscopic examination and reproducibly analyzed as a hexahydrate. The crystallographically characterized octahydrate[6] presumably resulted from somewhat different crystallization conditions. The chloride salt could be converted to the PF$_6$$^-$ salt, [Rh$_2$b$_4$Cl$_2$](PF$_6$)$_2$·2H$_2$O, by metathesis with NH$_4$PF$_6$ in 1 N HCl(aq). All compounds gave satisfactory elemental analyses; data are given in the supplementary material.

[Rh$_2$b$_4$Br$_2$]Br$_2$·2H$_2$O was prepared as a sparingly soluble orange precipitate by addition of concentrated aqueous NaBr to a concentrated 1 N H$_2$SO$_4$(aq) solution of [Rh$_2$b$_4$Cl$_2$]Cl$_2$·6H$_2$O.

[Rh$_2$b$_4$I$_2$](I$_3$)$_2$ was provided by N. S. Lewis.

The salts [Rh$_2$(TMB)$_4$X$_2$](PF$_6$)$_2$ (X = Cl, Br) were prepared by adding the appropriate dihalogen to a concentrated solution of [Rh$_2$-(TMB)$_4$](PF$_6$)$_2$ in CH$_3$OH. After precipitation with ether, the yellow solids were twice recrystallized from CH$_3$CN/ether. Elemental analyses for the analogous red iodide indicated a persistent triiodide impurity; the pure mixed salt [Rh$_2$(TMB)$_4$I$_2$](I$_3$)(PF$_6$) was easily obtained by employing excess I$_2$ in the preparation. The PF$_6$$^-$ anions of all of these salts are slowly hydrolyzed by moist air.

The salts [Rh$_2$(TMB)$_4$X$_2$](BPh$_4$)$_2$ (X = Br, I) were obtained from the PF$_6$$^-$ salts by metathesis with NaBPh$_4$ in methanol.

Dihalogen oxidation of a methanol solution of [Rh$_2$(TMB)$_4$]SO$_4$ (prepared in solution by mixing stoichiometric amounts of Ag$_2$SO$_4$ and [Rh$_2$(TMB)$_4$]Cl$_2$, and filtering off AgCl), followed by ether precipitation, yielded "sulfate" salts of the Rh$_2$(TMB)$_4$X$_2$$^{2+}$ cations. Elemental analysis of the red I$_2$ product is in fair agreement with a formulation [Rh$_2$-(TMB)$_4$I$_2$](HSO$_4$)$_2$·2H$_2$O, and electronic absorption extinction coefficients agree with those of other salts if this formula weight is assumed. Reproducible elemental analyses could not be obtained for the hygroscopic products from Br$_2$ and Cl$_2$ oxidations.

Solutions of Rh$_2$b$_4$(OH$_2$)$_2$$^{4+}$ in 1 N H$_2$SO$_4$(aq) could be prepared quantitatively either by precipitation of chloride with Ag$_2$SO$_4$ from solutions of [Rh$_2$b$_4$Cl$_2$]Cl$_2$·6H$_2$O or by Ce^{4+} oxidation[4a] of solutions of Rh$_4$b$_8$(OH$_2$)$_2$$^{6+}$. Halide precipitation with silver salts was also used to prepare solutions of Rh$_2$(TMB)$_4$(OH$_2$)$_2$$^{4+}$ in 1 N H$_2$SO$_4$(aq) and of the CH$_3$CN complex in CH$_3$CN solution.

Preparation of [Ir$_2$(TMB)$_4$](BPh$_4$)$_2$: In a typical synthesis, 0.1 g of[18] [IrCl(COD)]$_2$ and 0.1 g of TMB were dissolved in acetonitrile in separate beakers in a glovebox. Both solutions were filtered and the TMB solution was slowly added to the iridium-containing solution; the mixture was allowed to stir for ~15 min at which time the solvent and COD were pumped-off. The resulting metallic-colored solid was then dissolved in methanol and a filtered methanol solution of 0.11 g of sodium tetraphenylborate was added, resulting in the immediate precipitation of a turquoise solid. The air-sensitive solid could be recrystallized from either acetone or acetonitrile. The properties of this emissive Ir^I dimer will be discussed in detail elsewhere.

Preparation of [Ir$_2$(TMB)$_4$X$_2$](BPh$_4$)$_2$ (X = Cl, Br, I): An acetonitrile solution containing 0.05 g of [Ir$_2$(TMB)$_4$](BPh$_4$)$_2$ was titrated with an acetonitrile solution of X$_2$ until the blue color disappeared. The solvent was removed and the resulting yellow solid was slurried in methanol and

then filtered; the accumulated solid was collected and a solution containing 0.05 g of sodium tetraphenylborate was then added to the filtrate, and the precipitate that formed was filtered and collected. The two solids were combined and then crystallized from acetonitrile.

Spectroscopic Measurements. Thin optical quality crystals of [Rh$_2$-(TMB)$_4$Cl$_2$](PF$_6$)$_2$ were grown by slow evaporation of concentrated solutions in CH$_3$CN/toluene mixtures on quartz disks, balanced on edge in crystallization dishes. The only well-developed crystal face obtained was strongly dichroic (dark yellow/very light yellow). Suitable crystals, roughly estimated to have thicknesses of 10–30 μm, were masked off with (heat-conducting) copper grease and used for polarized single-crystal spectra. One such crystal was chipped off the disk and mounted on a glass fiber; the crystal face and orientation were determined from oscillation and Weissenberg X-ray photographs.

Crystals of [Rh$_2$(TMB)$_4$I$_2$](BPh$_4$)$_2$ were similarly grown from acetone solution. Two different well-developed faces were observed. One, while showing sharp extinctions, had negligible dichroism and a yellow transmittance. The second, more common, face type were strongly dichroic, one extinction showing yellow transmittance. The crystals were opaque for the other extinction, showing a greenish metallic reflectance. A few small, very thin specimens showed dark red transmittance for this extinction. Spectra were measured for both face types.

Variable-temperature solution measurements on Rh$_2$b$_4$Cl$_2$$^{2+}$ employed a 1:1 mixture of saturated aqueous LiCl and 1 M HCl (aq). This solvent mixture reproducibly forms glasses stable to liquid helium temperature and contracts very little (2.5%) from room temperature. Low-temperature spectra were corrected for solvent contraction.

Samples of [Rh$_2$(TMB)$_4$Cl$_2$](PF$_6$)$_2$, [Rh$_2$(TMB)$_4$I$_2$](BPh$_4$)$_2$, [Ir$_2$-(TMB)$_4$I$_2$](BPh$_4$)$_2$, and Mn$_2$(CO)$_{10}$ dissolved in poly(methylmethacrylate) (PMM) were obtained by slow evaporation of concentrated CH$_2$Cl$_2$ solutions of PMM and the complex on quartz plates. The evaporation was done in a loosely covered desiccator, the bottom of which was filled with CH$_2$Cl$_2$. Clear homogeneous regions of the films were masked off with black tape and used for electronic absorption measurements.

Preparation of KBr pellets containing Mn$_2$(CO)$_{10}$ was complicated by the volatility of the compound. In practice, optimal concentrations were arrived at by trial and error.

Far-infrared spectra of petroleum jelly mulls pressed between polyethylene plates were measured on a Perkin-Elmer 180 spectrophotometer. Laser Raman spectra were measured as described previously.[19] Depolarization ratios (ρ) were obtained by rotation of the polarization of the laser beam by 90°. Thus, with analysis of perpendicular scattering, theoretical values of ρ in D_{4h} for depolarized, parallel (single axis) polarized, and perpendicular polarized vibrations are[20] respectively 6/7, 1/2, and 2/9.

Results and Discussion

Vibrational Spectra. Figures 1 and 2 depict selected far-infrared spectra of the complexes. Variation of the axial halide reveals

(18) Herde, J. L.; Lambert, J. C.; Seroff, C. V. *Inorg. Synth.* **1974**, *15*, 18.

(19) Loehr, T. M.; Keyes, W. E.; Pincus, P. A. *Anal. Biochem.* **1979**, *96*, 456.

(20) Hester, R. E. In "Raman Spectroscopy"; Szymanski, H. A., Ed.; Plenum Press: New York, 1967; Chapter 4.

Properties of Metal–Metal Single Bonds

J. Am. Chem. Soc., Vol. 107, No. 26, 1985 7927
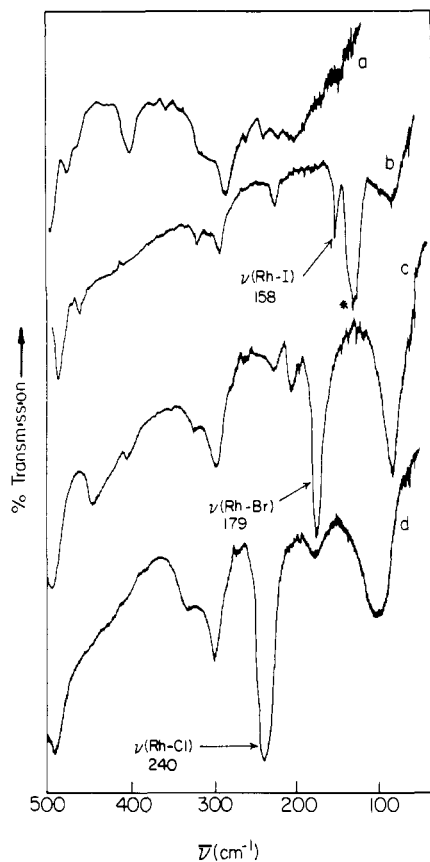
Figure 1. Far-infrared spectra: (a) $[Rh_2b_4](BPh_4)_2$; (b) $[Rh_2b_4I_2](I_3)_2$ (the asterisked band is due to I_3^-); (c) $[Rh_2b_4Br_2]Br_2 \cdot 2H_2O$; (d) $[Rh_2b_4Cl_2]Cl_2 \cdot 6H_2O$.
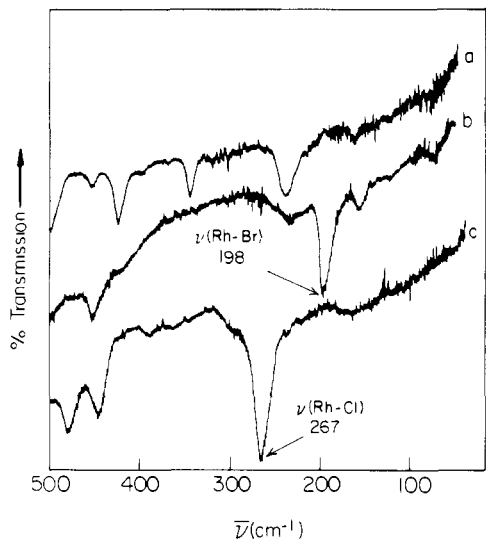
Figure 2. Far-infrared spectra: (a) $[Rh_2(TMB)_4](PF_6)_2$; (b) $[Rh_2(TMB)_4Br_2](PF_6)_2$; (c) $[Rh_2(TMB)_4Cl_2](PF_6)_2$.

one intense halide-sensitive band that is attributable to rhodium–halide stretching. Observed frequencies (ν_3) are given in Table II. They are ~ 70 cm^{-1} higher than reported[16] values for $Rh_2(O_2CR)_4X_2^{2-}$ complexes, consistent with axial halide–metal bond lengths that are about 0.2 Å shorter.[16] A firm assignment of ν_3 could not be made for $Rh_2(TMB)_4I_2^{2+}$, as several comparably intense bands appeared in the 100–200 cm^{-1} region for all salts investigated. We make no attempt to assign the numerous other absorption features; Boorman et al.[21] have suggested detailed

(21) Boorman, P. M.; Craig, P. J.; Swaddle, T. W. *Can. J. Chem.* **1970**, *48*, 838.
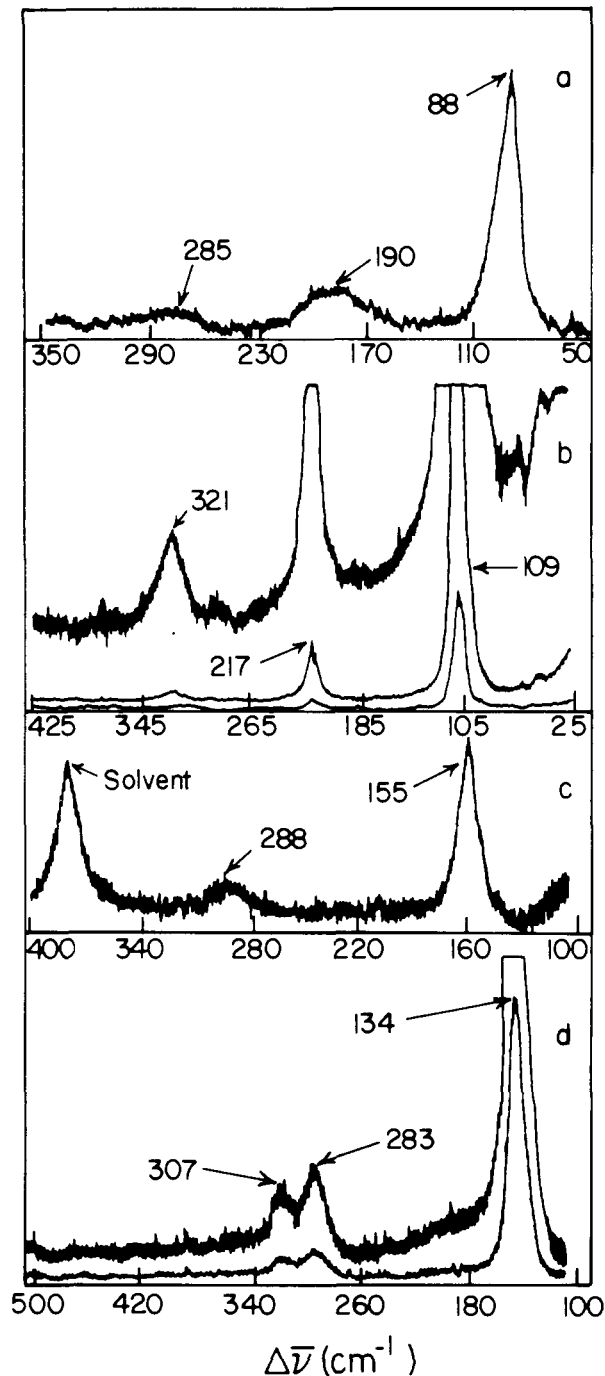
Figure 3. Raman spectra (647.1-nm excitation): (a) solid $[Rh_2b_4I_2](I_3)_2$; (b) solid $[Rh_2b_4Br_2]Br_2 \cdot 2H_2O$; (c) $[Rh_2(TMB)_4Cl_2](PF_6)_2$, 5×10^{-2} M in CH_3CN; (d) $[Rh_2b_4Cl_2]Cl_2 \cdot 6H_2O$, 5×10^{-2} M in 8 M HCl(aq).

assignments for related compounds.

Representative Raman spectra are shown in Figures 3 and 4, and the observed frequencies are included in Table II. While the compounds are completely nonabsorbing at the exciting wavelength, 647.1 nm, the spectra are extremely simple, just two or three intense low-frequency lines. Evidently there is strong and selective preresonance enhancement deriving from the intense near-UV electronic absorption bands. Preresonance enhancement of $\nu(Mn_2)$ was observed earlier for $Mn_2(CO)_{10}$.[22] Very similar spectra were obtained by using the 488.0 and 514.5 nm argon ion laser lines, but photodecomposition occurred on prolonged exposure to the laser beam. For the Ir[11] compounds, which have higher energy absorption bands, no photodecomposition occurred upon 514.5-nm excitation.

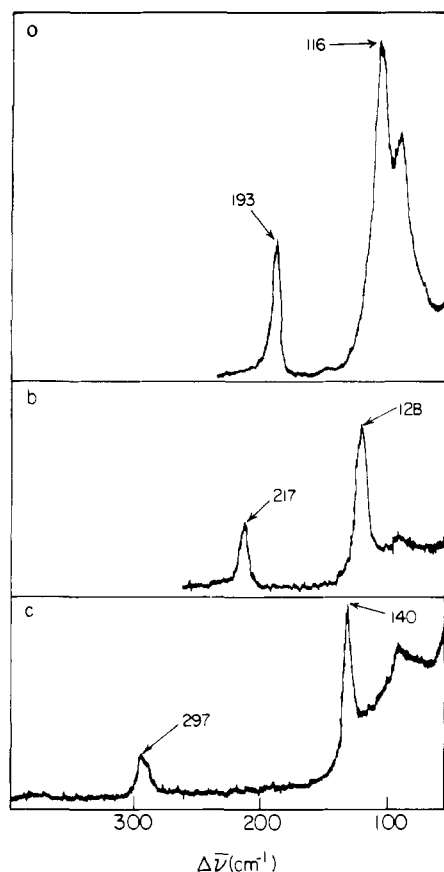(22) Quicksall, C. O.; Spiro, T. G. *Inorg. Chem.* **1970**, *9*, 1045.

Table III. One-Dimensional Force-Field Calculations. Frequencies Are Those Calculated with the Indicated Force Constants[a]

species	ν_1	ν_2	ν_3	$k_1 =$ $k(M_2)$	$k_2 =$ $k(M-X)$	k_{12}
$Rh_2b_4Cl_2{}^{2+}$	280	130	241	0.948	0.902	−0.090
$Rh_2(TMB)_4Cl_2{}^{2+}$	288	155	267	1.141	1.107	+0.029
$Rh_2b_4Br_2{}^{2+}$	217	107	179	0.913	0.849	+0.055
$Rh_2(TMB)_4Br_2{}^{2+}$	244	115	198	1.084	1.039	+0.033
$Rh_2b_4I_2{}^{2+}$	190	88	158	0.785	0.836	+0.106
$Ir_2(TMB)_4Cl_2{}^{2+}$	297	140	274	1.56	1.33	−0.135
$Ir_2(TMB)_4Br_2{}^{2+}$	217	128	196	1.62	1.28	+0.105
$Ir_2(TMB)_4I_2{}^{2+}$	193	116	149	2.09	1.05	+0.302

[a] ν in cm^{-1}; k in mdyn/Å.

Figure 4. Raman spectra (514.5-nm excitation) of $[Ir_2(TMB)_4X_2]$-$(BPh_4)_2$: (a) X = I; (b) X = Br; (c) X = Cl.

The complexes containing 1,3-diisocyanopropane all show a relatively weak Raman line near 300 cm^{-1}, which is insensitive to axial ligand. While this frequency is near the range appropriate to metal–carbon stretching and bending,[21,23] its absence in the spectra of the TMB complexes suggests assignment to a "ring deformation" mode of the rigid b–Rh_2 system, that is, to a mode composed of a complex mixture of ring stretching and bending coordinates. (Strictly analogous modes are well established for ethylenediamine–metal complexes.[24]) The depolarization ratio of this line measured for $Rh_2b_4Cl_2{}^{2+}$ in 8 M HCl(aq) with 647.1-nm excitation is 0.3 ± 0.05, indicating that the mode is totally symmetric but not purely axial.[20,25] For the more flexible ring system of the TMB complexes, the totally symmetric ring deformation(s) should be of lower frequency and may be broader and/or less coupled to axial modes.

Depolarization ratios for the other observed lines are all 0.5 ± 0.1, consistent with purely axial totally symmetric modes[20] (α_{xx} = α_{yy} ≃ 0). As preresonance enhancement is undoubtedly by axial (z) polarized electronic transitions (vide infra), which would[25] increase just α_{zz}, the axial purity of the modes is not strictly established by the ρ's. However, if mixing the axial and equatorial modes were significant, the equatorial modes should also be enhanced. As the structural data[3d,6–8] show C–Rh–Rh angles very near 90°, force field mixing of axial and equatorial modes should be very small.[26]

The frequencies of these lines are strongly sensitive to the axial ligand and therefore they are assigned to the two axial stretching

modes of the X–M–M–X unit (labeled ν_1 and ν_2 in Table II). The complex $Rh_2(TMB)_4Br_2{}^{2+}$ proved to be an exception in that three halide-sensitive lines were observed with two roughly equally intense lines near 100 cm^{-1}. Essentially the same spectrum was found for three different crystalline salts and also for solutions. Notably, 514.5-nm spectra of the solid $PF_6{}^-$ salt showed that both "ν_2" lines disappeared at the same rate as the sample photodecomposed, while a line at 172 cm^{-1} due to $Br_3{}^-$ photoproduct grew in. We suggest that a Fermi resonance is involved; an overtone of a Rh–Br bending mode might be responsible.[27]

Force-field calculations[28] were carried out assuming a linear X–M–M–X model, and derived force constants are given in Table III. Since interaction with rhodium–carbon and ring deformation modes has been neglected, the force constants are not reliable in a quantitative sense.[29] For the Rh dimers, it is encouraging that k_{12} values (k_{12} is an off-diagonal force constant), which should absorb deficiencies in the calculation, are reasonably small. With the exception of the iodide complex, which has a particularly large k_{12}, the complexes yield rhodium–rhodium stretching constants very near 1 mdyn/Å,[30] closely comparable to derived force constants for other compounds containing metal–metal single bonds.[31] Slightly larger force constants for the TMB complexes correlate with slightly shorter bond distances (Table I). While neither ν_1 nor ν_2 is a pure rhodium–rhodium stretch, ν_2 *approximates* one; most of the variation in ν_2 as a function of X is more simply modeled by changes in the reduced mass of "diatomic" $(XRh)_2$. The potential energy distributions (PED's) agree with this description of ν_2. The k_1's correspond to a "diatomic" Rh_2 stretching frequency of ∼180 cm^{-1}, which is close to the observed frequency (176 cm^{-1}) for $Rh_2b_4(OH_2)_2{}^{4+}$; we would expect that the light aquo ligand would have little effect on the rhodium–rhodium stretching frequency.

The results for the Ir^{II} compounds are somewhat less satisfactory, as seen from Table III. As an inevitable consequence of Ir^{II} frequencies being similar to those of analogous Rh^{II} compounds, the two diagonal force constants are considerably larger, since the Ir mass is larger. This is not in disagreement with the single structural datum available (Table I) which, as it indicates bond lengths nearly the same as those for Rh^{II}, would support stronger bonds in order to be consistent with the larger ionic radius of Ir. Although the k_{12} values for Ir complexes are all rather large (the iodide yields a PED indicating dominant metal–metal

(23) Swanson, B. I.; Jones, L. H. *Inorg. Chem.* **1974**, *13*, 313.

(24) (a) Krishnan, K.; Plane, R. A. *Inorg. Chem.* **1966**, *5*, 852. (b) Flint, C. D.; Matthews, A. P. *Inorg. Chem.* **1975**, *14*, 1219. (c) Stein, P.; Miskowski, V.; Woodruff, W. H.; Griffin, J. P.; Werner, K. G.; Gaber, B. P.; Spiro, T. G. *J. Chem. Phys.* **1976**, *64*, 2159. (d) Hakamata, K.; Urushiyama, A.; Degen, J.; Kupka, H.; Schmidtke, H. H. *Inorg. Chem.* **1983**, *22*, 3519.

(25) San Filippo, J.; Fagan, P. J.; DiSalvo, F. J. *Inorg. Chem.* **1977**, *16*, 1016.

(26) Bratton, W. K.; Cotton, F. A.; Debeau, M.; Walton, R. A. *J. Coord. Chem.* **1971**, *1*, 121.

(27) For Hg_2Cl_2, whose ν_1, ν_2, and ν_3 frequencies (270, 167, and ∼260 cm^{-1}) are very similar to those of $Rh_2(TMB)_4Cl_2{}^{2+}$, the ungerade and gerade bending frequencies are 110 and 42 cm^{-1}: Goldstein, M. *Spectrochim. Acta* **1966**, *22*, 1389.

(28) Hertzberg, G. "Infrared and Raman Spectra of Polyatomic Molecules"; Van Nostrand: New York, 1945; pp 188–189.

(29) Calculations have also been carried out for the Ir dimers with allowance for nonzero interaction force constants between the two Ir–X oscillators, and more reasonable force fields were obtained (ref 9). However, it is likely that neglect of the equatorial bridging ligands is too drastic an approximation to justify much further work along these lines. It should be noted that an analysis of bridging-ligand effects on the vibrational modes of Pt^{II} and Pt^{III} binuclear complexes has been published: Stein, P.; Dickson, M. K.; Roundhill, D. M. *J. Am. Chem. Soc.* **1983**, *11*, 2489.

(30) It is interesting that a calculation by Badger's rule (see: Herschbach, D. R.; Laurie, V. W. *J. Chem. Phys.* **1961**, *35*, 458) of the force constant for diatomic rhodium with a bond distance of 2.84 Å yields k = 1.0 mdyn/Å.

(31) Spiro, T. G. *Prog. Inorg. Chem.* **1970**, *11*, 7.

Table IV. Electronic Absorption Data for $Rh_2b_4L_2^{n+}$ ^{a}

L (n)	I	II
OH_2 (4)	24.1 (1250)	32.1 (33 600)
OH_2, Cl (3)^b	23.7 (1250)	31.1 (35 400)
Cl (2)	23.7 (1880)	29.7 (59 000)
Cl (2)^c	24.1 (2300)	29.2 (52 000)
Br (2)	~23 (~3700, sh)	27.5 (68 500)
I (2)^c	21.5 (23 000)	25.2 (62 000)
SCN (2)	–	25.1 (74 300)

^{a} Solvent is 1 N H_2SO_4(aq), except where noted: data are given as $\bar{\nu}_{max} \times 10^{-3}$ (cm^{-1}) (ϵ/Rh_2); dashed entry, no band observed. ^{b} Spectrum determined from Cl^- titration experiments, see text. ^{c} Solvent is CH_3CN.
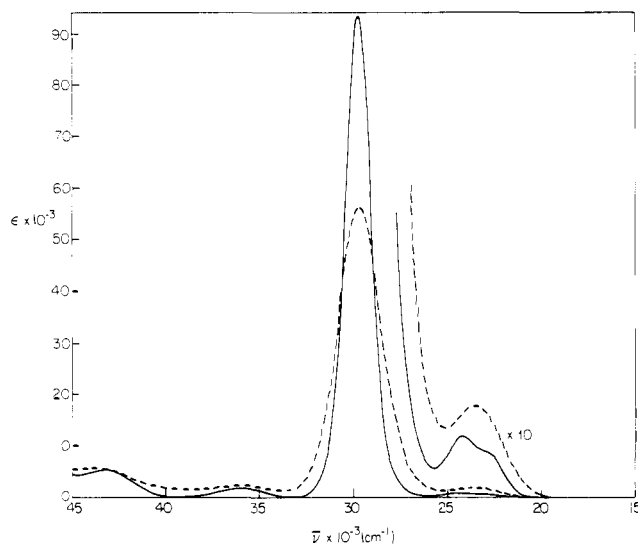

Figure 5. Electronic spectra of $Rh_2b_4Cl_2^{2+}$ in 1:1 saturated aqueous LiCl: 1 M HCl(aq) at 15 K (—) and 300 K (---).

character in ν_1 (!)),[29] the force fields for the chloride and bromide complexes appear to be reasonable, and $k(Ir–Ir) \simeq 1.6$ mdyn/Å is not inconsistent with literature data.[31]

The major conclusion from the vibrational spectral studies is that the complexes contain normal metal–metal single bonds that are reasonably independent of the axial ligand. The observed ν_2 is the $Rh^{II}–Rh^{II}$ or $Ir^{II}–Ir^{II}$ stretching frequency, with $k(Ir–Ir)$ (~1.6 mdyn/Å) > $k(Rh–Rh)$ (~0.9 to 1.1 mdyn/Å). For comparison, stretching frequencies are 79 and 55 cm^{-1} for respectively $Rh_2b_4^{2+}$ and $Rh_2(TMB)_4^{2+}$ in CH_3CN solution.[5,32] These frequencies correspond to "diatomic" $Rh^I–Rh^I$ force constants of only 0.1–0.2 mdyn/Å. An additional comparison of interest is to the triplet $d\sigma^*p\sigma$ excited state of $Rh_2b_4^{2+}$, which has $\nu(Rh_2) = 144$ cm^{-1} in CH_3CN solution,[5] corresponding to a diatomic force constant of 0.63 mdyn/Å.

Electronic Spectra. The electronic spectra of $Rh_2b_4Cl_2^{2+}$ in aqueous LiCl at room and low temperatures are shown in Figure 5; and Tables IV and V summarize room-temperature spectral data for complexes of $Rh_2b_4^{4+}$ and $M_2(TMB)_4^{4+}$ (M = Rh, Ir), respectively. The tables identify absorption bands in order of increasing energy with Roman numerals I through IV. Data for bands III and IV are not tabulated for the $Rh_2b_4^{4+}$ complexes. While these bands were evident in some spectra (notably Figure 5), spectra in aqueous solution required excess anions that usually mask the high-energy region; spectra for the TMB complexes in CH_3CN solution could be obtained in the absence of excess anions. However, BPh_4^- obscured the high-energy region for the Ir^{II} compounds, so the position of bands III and IV could not be measured.

With the exception of the iodide complexes, which will be discussed separately, the spectra are dominated by a single very intense, isolated band, labeled II in the tables. The oscillator
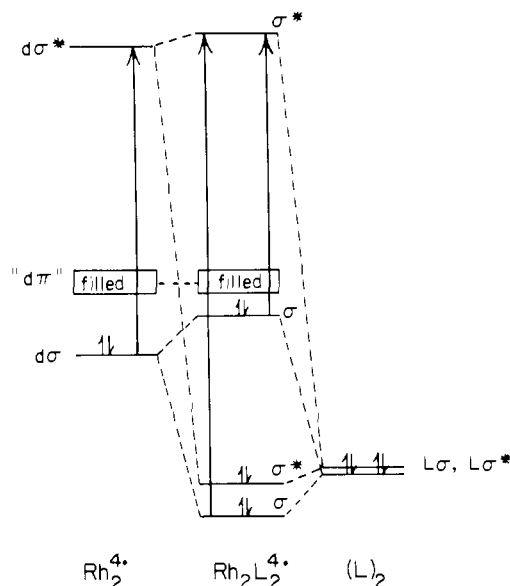

Figure 6. Molecular orbital diagram for interaction of Rh_2^{4+} with two σ-donor axial ligands. The $\sigma \rightarrow \sigma^*$ transitions are indicated by arrows.

strength (f) for the 337-nm (29 700 cm^{-1}) band of $Rh_2b_4Cl_2^{2+}$ was found to be 0.71, and it is independent of temperature. The analogous absorption band of the diaquo complex, while considerably broader, has a similar f (0.68). In general, the band becomes narrower and slightly more intense (in terms of f) as its energy decreases.

Such high f's signal a strongly allowed transition. Comparison to the $d\sigma \rightarrow d\sigma^*$ transition of $Mn_2(CO)_{10}$ at 29 240 cm^{-1} ($f = 0.32$)[11] suggests that we make a similar assignment. This is an $N \rightarrow V$ transition in the Mulliken notation[33] and should have an oscillator strength approaching 1 for a strong single bond. The lower oscillator strength for the $Mn_2(CO)_{10}$ transition could correlate to the rather long (2.90 Å)[10] metal–metal bond in this compound.

The $d\sigma \rightarrow d\sigma^*$ transition shifts systematically to lower energy with more reducing axial ligands. A correlation of $d\sigma \rightarrow d\sigma^*$ energy with metal–metal bond strength has been suggested[34] for axially substituted $M_2(CO)_{10}$ derivatives. While this also could be true for Rh^{II} complexes, the $Rh_2I_2^{2+}$ example (Table I) does not indicate any strong correlation with metal–metal bond length.

A reasonable explanation, as proposed previously,[2a] involves mixing of the metal–metal $d\sigma \rightarrow d\sigma^*$ transition with axial ligand-to-metal charge transfer (LMCT), $L\sigma \rightarrow d\sigma^*$. This is indicated by the orbital mixing in the diagram in Figure 6. For aquo and CH_3CN complexes, whose lone pair IP's are much higher than those of halides, we assume that CT mixing is negligible.

It should be noted that the d labels in Figure 5 are an oversimplification. Mixing of σ-symmetry d and p orbitals (d_{z^2} and p_z) is needed to account for the weak $Rh^I–Rh^I$ bond,[3b,5a] and nd mixing with $(n + 1)p$, $(n + 1)s$, and π^* ligand orbitals appears[35] to provide an important component of the bonding in a long[16] metal–metal single bond such as that of $Mn_2(CO)_{10}$. But d orbitals are the largest contributors to those MO's,[11,35] so we retain d labels for simplicity.

Given the reasonable assumption that axial ligand mixing of σ-symmetry combinations (which are closer in energy) will be greater than that of σ^* combinations, the lowest energy $d\sigma \rightarrow d\sigma^*$ transition should red shift. Note that a second allowed $\sigma \rightarrow \sigma^*$ transition, predominantly LMCT according to Figure 6, should fall at higher energy. According to Mulliken,[33] mixing in this

(32) (a) Dallinger, R. F., unpublished work. (b) Loehr, T. M.; Miskowski, V. M., unpublished work.

(33) Mulliken, R. S. *J. Chem. Phys.* **1939**, *7*, 21, 121.
(34) (a) Jackson, R. A.; Poë, A. *Inorg. Chem.* **1978**, *17*, 997. (b) Poë, A. J.; Jackson, R. A. *Inorg. Chem.* **1978**, *17*, 2330.
(35) (a) Brown, D. A.; Chambers, W. J.; Fitzpatrick, N. J.; Rowlinson, R. M. *J. Chem. Soc. A* **1971**, 720. (b) Elian, M.; Hoffmann, R. *Inorg. Chem.* **1975**, *14*, 1058. (c) Heijser, W.; Baerends, E. J.; Ros, P. *Symp. Faraday Soc.* **1980**, *14*, 211.

Table V. Electronic Absorption Data for $M_2(TMB)_4L_2^{n+}$ Complexes[a]

L(solvent) (n)	I	II	III	IV
M = Rh^{II}				
CH$_3$CN(CH$_3$CN) (4)	23.8 (960)	32.5 (38 600)	–	–
H$_2$O (1 N H$_2$SO$_4$(aq)) (4)	24.7[b]	32.2[b]	–	–
Cl (1 N H$_2$SO$_4$(aq)) (2)	24.2 (1700)	30.6 (55 400)	36.4 (2200)	43 (4000, sh)
Cl(CH$_3$CN) (2)	24.4 (2500)	30.0 (55 500)	35.1 (3300)	43 (3300, sh)
Br (1 N H$_2$SO$_4$(aq)) (2)	24 (3800, sh)	28.3 (58 000)	–	–
Br(CH$_3$CN) (2)	24 (4500, sh)	27.8 (60 000)	33.1 (4700)	41 (1800, sh)
I(CH$_3$CN) (2)	21.7 (22 000)	25.4 (55 200)	31.4 (8200)	41 (10 000, sh)
M = Ir^{II}				
Cl(CH$_3$CN) (2)	28.6 (5910)	36.5 (50 500)	–	–
Br(CH$_3$CN) (2)	30.3 (4510)	33.7 (52 600)	–	–
I(CH$_3$CN) (2)	26.7 (8100, sh)	30.3 (49 800)	–	–

[a] Data are given as $\nu_{max} \times 10^{-3}$ (cm^{-1}) (ϵ/M_2); dashed entries, not measured. [b] ϵ not determined.

"conjugated" system should tend to concentrate all of the oscillator strength into the lower energy transition, which accounts for the intensity effects. Since M–M and M–X bond orders are closely comparable in these complexes, mixing is extensive. It is interesting that mixing appears to be much smaller for the $d\sigma \rightarrow d\sigma^*$ transitions of Rh$_2$(O$_2$CCH$_3$)$_4$X$_2^{2-}$ complexes,[16] which have much weaker bonds to the axial ligands. A detailed theoretical description of an extreme example of such mixing[14] shows that it does correspond to metal–metal bond weakening. Thus, the effects observed for M$_2$(CO)$_{10}$ derivatives[34] may have a similar explanation; the axial ligands in that case were phosphines, which optically are very reducing.[36]

The $d\sigma \rightarrow d\sigma^*$ absorption maxima occur at slightly higher energies (100–1000 cm^{-1}) for Rh$_2$(TMB)$_4^{4+}$ complexes than for Rh$_2$b$_4^{4+}$ analogues, which correlate with decreasing Rh^{II}–Rh^{II} bond lengths (Table I). However, the band shifts are not dramatic; indeed, solvent shifts, with the $d\sigma \rightarrow d\sigma^*$ maximum at lower energy in CH$_3$CN than in H$_2$O, are comparable to these shifts. There is an interesting difference in kinetic behavior; the exchange of axial ligands occurs within the mixing time in H$_2$O but is relatively slow (half-lives of the order of several hours) in CH$_3$CN. We suggest that both the absorption shifts and the difference in kinetic behavior are compatible with strong hydrogen bonding of the anionic axial ligands to solvent water. Such H bonding was observed in the crystal structure[6] of [Rh$_2$b$_4$Cl$_2$]Cl$_2$·8H$_2$O, and the observed Rh–Cl bond lengths (Table I) are rather long, which would enhance the tendency to H bond.

Absorption data for Rh$_2$b$_4$Cl(OH$_2$)$^{3+}$ in Table IV derive from a study of the equilibria involving Rh$_2$b$_4$(OH$_2$)$_2^{4+}$ and Cl$^-$ in 1 N H$_2$SO$_4$(aq). (For the first chloride, log K = 4.3 with an isosbestic point at 318 nm; for the second chloride, log K = 3.2 with an isosbestic point at 326 nm.) Qualitatively, we have found that the formation constants for bromide complexes are considerably higher, so Rh$_2$b$_4^{4+}$ is a soft acid.

Also notable in Figure 5 is the remarkable decrease of the $d\sigma \rightarrow d\sigma^*$ bandwidth with decreasing temperature. Qualitatively similar behavior was observed for Rh$_2$(TMB)$_4$Cl$_2^{2+}$ in a PMM matrix, though a considerably broader $d\sigma \rightarrow d\sigma^*$ transition was found; this is largely a matrix effect, as the bandwidths were similar for Rh$_4$b$_4^{4+}$ and Rh$_2$(TMB)$_4^{4+}$ complexes in common solvents.

Such drastic thermal effects are now considered[11,37] to be characteristics of metal–metal $d\sigma \rightarrow d\sigma^*$ transitions. They have been attributed[11] to the large Franck–Condon factors the transition should have for the low-frequency (hence, thermally accessible) metal–metal stretch. Spectra in a PMM matrix for Mn$_2$(CO)$_{10}$ show effects similar to those previously noted[11] for glassy solutions (Figure 7). A similar temperature dependence was exhibited in spectra of KBr pellets of Mn$_2$(CO)$_{10}$ (not shown). The latter spectra should be characteristic of the crystal[10] and tend to exclude
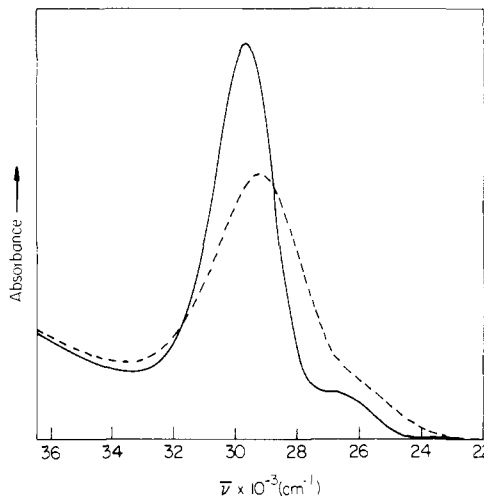
Figure 7. Electronic absorption spectra of Mn$_2$(CO)$_{10}$ in PMM film at 23 K (—) and 300 K (- - -).

the possibility that rotation about the metal–metal bond might be responsible for the temperature dependence.

We have attempted to quantify the temperature effect by a moment analysis.[38] For an allowed transition the zeroth moment (proportional to oscillator strength) is temperature independent. Parameters of interest related to the first and second moments are the normalized first moment, or average of the distribution, and the normalized second central moment[38] (m^2). For a Gaussian band (a good approximation for all the examples we will consider), the first moment is simply the maximum, $\bar{\nu}_{max}$, while m^2 is related to the half-width ($\Delta^{1/2}$) by eq 1.

$$m^2 = (8 \ln 2)^{-1}(\Delta^{1/2})^2 \tag{1}$$

Assuming that the ground state is a harmonic oscillator, theory[38] predicts that both $\bar{\nu}_{max}$ and m^2 should have temperature dependences of the form given by eq 2. Here k is the Boltzmann

$$\sum_i A_i \coth\left(\frac{\hbar\omega_i}{2kT}\right) + B \tag{2}$$

constant, A_i and B are constants, and the $\hbar\omega_i$ values are Franck–Condon-active ground-state vibrational frequencies.

Second-moment and first-moment plots for Mn$_2$(CO)$_{10}$, Rh$_2$b$_4$Cl$_2^{2+}$, and Rh$_2$(TMB)$_4$Cl$_2^{2+}$ are shown in Figures 8 and 9. (A second-moment plot for Mn$_2$(CO)$_{10}$ in KBr is not given, because Beer's law is not strictly valid for such samples.) The lines are best fits to eq 2, and the parameters are summarized in Table VI; for the second-moment fits, eq 1 was used to convert the

(36) Miskowski, V. M.; Robbins, J. L.; Hammond, G. S.; Gray, H. B. *J. Am. Chem. Soc.* **1976**, *98*, 2477.

(37) (a) Wrighton, M. S.; Ginley, D. S. *J. Am. Chem. Soc.* **1975**, *97*, 4246. (b) Abrahamson, H. B.; Frazier, C. C.; Ginley, D. S.; Gray, H. B.; Lilienthal, J.; Tyler, D. R.; Wrighton, M. S. *Inorg. Chem.* **1977**, *16*, 1554. (c) Tyler, D. R.; Levenson, R. A.; Gray, H. B. *J. Am. Chem. Soc.* **1978**, *100*, 7888.

(38) A comprehensive treatment of band shape moment analysis is given in the following: Markham, J. J. *Rev. Mod. Phys.* **1959**, *31*, 956. A brief but lucid treatment is given in the following: Ballhausen, C. J. "Molecular Electronic Structures of Transition Metal Complexes"; McGraw-Hill; New York, 1979; pp 132–135.
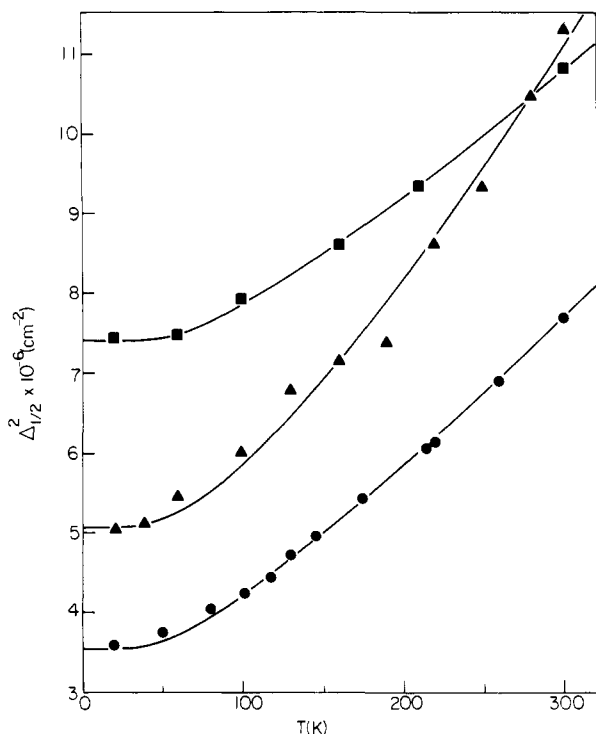
Figure 8. Second-moment plots for $d\sigma \rightarrow d\sigma^*$ bands: (O) $Rh_2b_4Cl_2^{2+}$ in LiCl(aq) glass; (□) $Rh_2(TMB)_4Cl_2^{2+}$ in PMM; (△) $Mn_2(CO)_{10}$ in PMM. The lines are calculated from the parameters in Table VII.
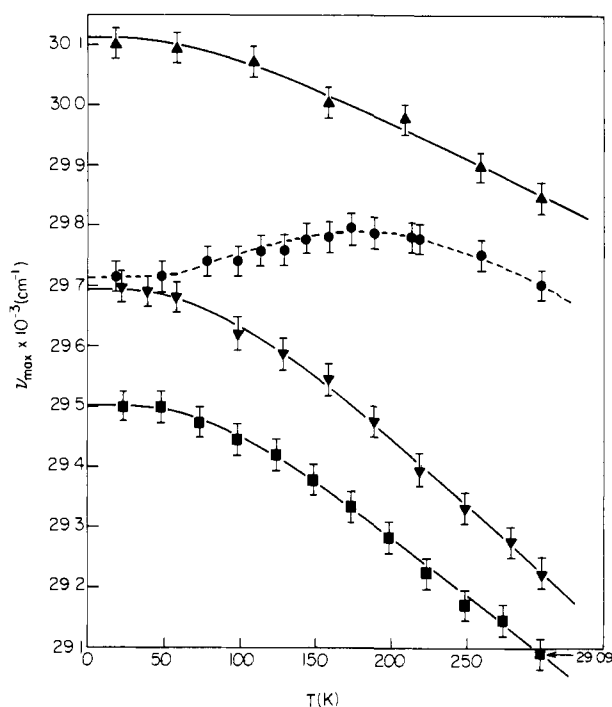
Figure 9. First-moment plots for $d\sigma \rightarrow d\sigma^*$ bands: (O) $Rh_2b_4Cl_2^{2+}$ in LiCl(aq) glass; (△) $Rh_2(TMB)_4Cl_2^{2+}$ in PMM; (▽) $Mn_2(CO)_{10}$ in PMM; (□) $Mn_2(CO)_{10}$ in KBr. The lines are calculated from the parameters in Table VII, except for the dashed line through the ● points, which is solely a marker.

parameters to those for m^2, and these are the ones tabulated. First-moment data for $Rh_2b_4Cl_2^{2+}$ do not fit eq 2.

We emphasize that in the tabulated fits we assumed a single active $\hbar\omega$, which was taken to be that of the known metal–metal stretching frequency; values for the rhodium complexes (ν_2) are given in Table II, whereas that of $Mn_2(CO)_{10}$ is[22] 160 cm^{-1}. The major conclusion is thus that the metal–metal stretch adequately accounts for the temperature dependence. Nonlinear least-squares

Table VI. Best-Fit First-Moment ($\bar{\nu}_{max}$) and Second-Moment (m^2) Parameters[a]

	1st moment (cm^{-1})		2nd moment (cm^{-2})		$\hbar\omega$ (cm^{-1})
	A	B	A	B	
$Rh_2b_4Cl_2^{2+}$, LiCl(aq)	b	b	3.39×10^5	3.01×10^5	135
$Rh_2(TMB)_4Cl_2^{2+}$, PMM	−142	30 250	3.34×10^5	1.00×10^6	155
$Mn_2(CO)_{10}$, PMM	−271	29 960	6.10×10^5	3.12×10^5	160
$Mn_2(CO)_{10}$, KBr	−240	29 740	c	c	160

[a] See text for discussion. [b] Data do not fit coth equation. [c] Fit not attempted.

fits to the three parameters $\hbar\omega$, A, and B yield similar $\hbar\omega$'s, but with large uncertainties because of correlations among the parameters. However, adequate fits to eq 1 and 2 cannot be obtained for $\hbar\omega$'s differing from $\nu(M_2)$ by greater than ±20%. Given the limited set of plausibly active $\hbar\omega$'s (Table II), the assignment of $\nu(M_2)$ as the thermally important Franck–Condon active mode seems secure. With $\hbar\omega$ fixed, the fits reduce to linear least squares, and the A and B values of Table VI were obtained in this way. The worst fit, the second moment data for $Mn_2(CO)_{10}$ in PMM, has a linear correlation coefficient of 0.987.

According to harmonic oscillator theory,[38] the coefficients yield information on excited-state properties. For the m^2 fits, A is predicted to be $S(\hbar\omega_e)^2$, where $\hbar\omega_e$ is the excited-state vibrational frequency and S is the dimensionless Huang–Rhys parameter.[39] S is related to the excited-state distortion ΔQ by eq 3,[38,40] where

$$S = \left(\frac{\mu\omega_e}{2\hbar\omega_g}\right)\Delta Q^2 \qquad (3)$$

$\hbar\omega_g$ is the ground-state vibrational frequency and μ is the reduced mass. (For equal ground- and excited-state frequencies, S is[39] the ratio of the vibronic (1,0) and (0,0) intensities, or for large S, the value of the excited-state vibrational quantum number at which the transition reaches maximum intensity.)

If we take the excited-state vibrational frequency to be 135 cm^{-1}, which is the ground-state value for $Rh_2b_4Cl_2^{2+}$, then the value found for A implies $S = 18.6$, and the calculated ΔQ is 0.42 Å. It would seem to be more reasonable[41,42] to assume the excited-state frequency to be 80 cm^{-1}, the value for[5] ground-state $Rh_2b_4^{2+}$ (with, formally, no metal–metal bond), as molecular models suggest that the bridging ligand cannot accommodate Rh–Rh distances longer than $\sim$3.3 Å. Then, the calculated S and ΔQ are 53 and 1.21 Å, whereas ΔQ between the ground states of $Rh_2b_4Cl_2^{2+}$ and $Rh_2b_4^{2+}$ is 0.41 Å.

Clearly, sensible values are not obtained for all the calculated parameters. The problem is that the theory assumes harmonic oscillators. For such large distortions, even very small anharmonicities would be of consequence, since the band-shape analysis involves transitions over a very wide range of vibrational quantum number. Explicit calculations[43] assuming a Morse potential for the excited state confirm that the harmonic theory is grossly inadequate for such cases. For the present, we simply conclude that the results do require a large distortion along the metal–metal coordinate, consistent with the view of the transition as a metal–metal $d\sigma \rightarrow d\sigma^*$ process. The considerably larger A term for $Mn_2(CO)_{10}$ (Table VI) suggests a larger distortion and may be consistent with the unbridged structure.

Simple theory also fails in the interpretation of the A terms for the first-moment temperature dependence (Table VI). The

(39) Huang, K.; Rhys, A. *Proc. R. Soc. (London)* **1958**, *A204*, 406.
(40) S here is a "generalized" S defined by Markham (ref 38, p 978).
(41) Although the triplet $d\sigma \rightarrow d\sigma^*$ state is dissociative and the "ionic"[33,42] $d\sigma \rightarrow d\sigma^*$ singlet could become dissociative by interaction with other states of the same ($^1A_{2u}$) symmetry, neither state of the Rh^{II} complexes leads to net metal–metal dissociation, because of the four bridging diisocyanide ligands.
(42) Coulson, C. A.; Fischer, I. *Philos. Mag.* **1949**, *40*, 386.
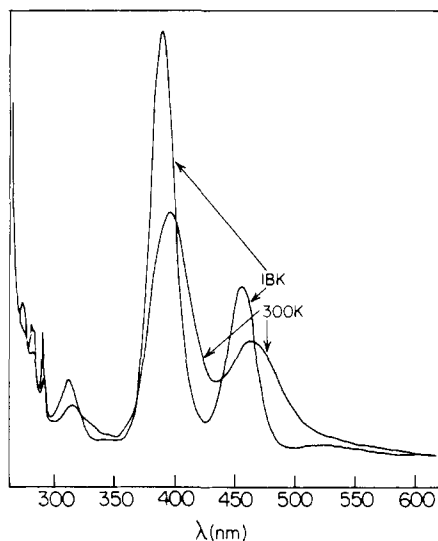
Figure 10. Electronic spectrum of a PMM film of [Rh₂(TMB)₄I₂]-(BPh₄)₂ at 18 K (—) and 300 K (---). A trace of Rh₂(TMB)₄²⁺, due to reduction by the polymer matrix in the course of forming the film, is responsible for the weak band at ~520 nm and some of the absorption at 312 nm. The sharp spikes below 300 nm are anion phenyl absorption.

most negative value possible for these terms in a harmonic oscillator model[38] is $-\hbar\omega_g/4$ (requiring the dubious assumption that the excited-state frequency is zero). Our theoretical analysis[43] suggests that the observed values are dominated by cross terms $\Delta Q \delta q$, where δq is the change in average ground-state internuclear distance over the observed temperature range. The δq is due to ground-state anharmonicity and can be shown[43] to be proportional to coth $(\hbar\omega_g/2kT)$ for small anharmonicity. There is spectroscopic[44] and X-ray structural[10] evidence for anharmonicity of ν(M–M) for Mn₂(CO)₁₀, as indicated by significant decrease of both ν(M₂) and d(M₂) at low temperature. The main point is that these terms will be very small unless ΔQ, the excited-state distortion along the M–M coordinate, is very large, so the large observed values of the first-moment A term again provide evidence for large excited-state distortion.

The variation of $\bar{\nu}_{max}$ for Rh₂b₄Cl₂²⁺ is very small and does not follow a coth law (Figure 9). Such small effects are usually attributed to "lattice expansion",[38,45] and it is likely that thermally discontinuous effects in[45] the LiCl(aq) matrix have overpowered the weak "Franck–Condon" effects.

The temperature-independent B terms (Table VI) deserve comment. Those for the first moments are related to the electronic transition energies, but simple diatomic theory[38] does not predict nonzero B terms for the normalized second central moments. However, nonzero B terms have been noted previously,[38,46] and eq 2 suggests that they could be attributed to A terms of Franck–Condon-active vibrations that are too energetic to contribute strongly to the temperature dependence. For Rh₂b₄Cl₂²⁺, the Raman-active modes at 283 and 307 cm⁻¹ (Table III) are such vibrations, and their preresonance enhancement implies that they do have significant Franck–Condon factors for dσ → dσ*. An additional contributor would be inhomogeneous broadening, which, as previously noted, appears to affect the width of the dσ → dσ* band of Rh₂(TMB)₄Cl₂²⁺ in a PMM matrix. It is encouraging that while the B term for this sample is very large (Table VI), eq 2 still fits the data, and the derived A term for ν(Rh₂) is nearly identical with that for Rh₂b₄Cl₂²⁺.

Spectra of Rh^II complexes with axial iodide ligands are anomalous in the sense that they exhibit two very intense bands (Figure 10). Clearly, both bands display the drastic thermal effects[47]
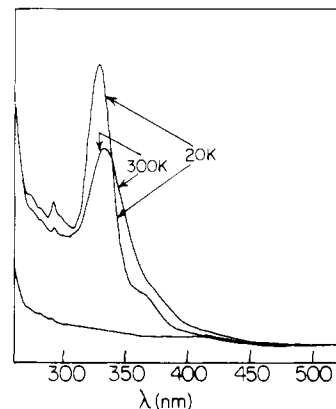
Figure 11. Electronic spectrum of a PMM film of [Ir₂(TMB)₄I₂](BPh₄)₂ at 20 K (—) and 300 K (---).

that are associated with dσ → dσ* transitions.

Single-crystal spectra of [Rh₂(TMB)₄I₂](BPh₄)₂ (see Experimental Section) show that there is one crystal face in which both bands appear only weakly, independent of polarization; and there is a second face for which both appear only weakly for one extinction. This polarization behavior can only be understood if both bands are identically polarized along a single axis that is perpendicular to the crystal face that absorbs weakly (independent of light polarization). We have not determined the crystal structure of this material, but we have determined the structure[9] of [Ir₂(TMB)₄I₂](BPh₄)₂, which was crystallized from the same solvent (acetone). This latter crystal is orthorhombic, *Pccn*, and the I₂Ir₂ units are rigorously parallel to the crystallographic c axis. If the rhodium complex is isomorphous, as seems very likely, then the observed polarization behavior is consistent with the weakly absorbing face being (001); accordingly, both bands are inferred to be polarized along the Rh–Rh axis.

Additional information derives from the spectrum of the analogous Ir^II complex (Figure 11). The Ir^II complexes exhibit spectra (Table VI) similar to those of Rh^II, but somewhat blue-shifted. The blue-shift of the metal–metal dσ → dσ* is consistent with a slightly stronger M–M bond, as suggested by the vibrational data (vide supra). Importantly, the Ir₂(TMB)₄I₂²⁺ complex has a "normal" spectrum, with a single strong dσ → dσ* band. As LMCT transitions are known[48] to occur at much higher energies for Ir complexes than for Rh complexes, we suggest that very strong charge-transfer mixing accounts for the peculiarities of the Rh₂I₂²⁺ spectra. Indeed, Rh(n-C₄H₉NC)₄I₂⁺ exhibits[49] an intense LMCT absorption at 387 nm (ϵ = 11 200), suggesting that Iσ → dσ* and Rh–Rh dσ → dσ* transitions should fall in the same energy region. We therefore attribute the two intense bands in the Rh₂(TMB)₄I₂²⁺ spectrum (Figure 9) to these strongly mixed transitions. In this interpretation, neither band of the Rh^II complex can be assigned to pure metal–metal dσ → dσ*. This is an extreme case of LMCT mixing, as alluded to earlier.

The weak absorptions observed for the Rh^II and Ir^II complexes (band I of Tables IV and V) are analogous to the "dπ" → dσ* absorption system of Mn₂(CO)₁₀ (Figure 7). In the D_{4h} symmetry of Rh₂b₄Cl₂²⁺, the "dπ" orbitals (d_{xy}, d_{xz}, d_{yz}) on each Rh form bonding and antibonding molecular orbitals of π and δ symmetries relative to the metal–metal interaction. The energy ordering calculated[16a] for Rh₂(O₂CCH₃)₄(OH₂)₂ is δ* > π* ≫ δ > π. Distortion to D_4 by torsion about the metal–metal bond, as in the case[7] of Rh₂(TMB)₄Cl₂²⁺, mixes π and π*, whereas δ* and δ become degenerate in the D_{4d} limit. The total "dπ" splitting of (D_{4d}) Mn₂(CO)₁₀ is ~5000 cm⁻¹ according to photoelectron spectra.[50,51] In D_{4h} symmetry, the only allowed transition to σ*

(43) Miskowski, V. M., unpublished work.

(44) Prasad, P. N. *Spectrochim. Acta* **1977**, *33A*, 335.

(45) Ivey, H. F. *Phys. Rev.* **1947**, *72*, 341. The glass transition temperature of 9 M LiCl(aq) is 143 K (Angell, C. A.; Sore, E. J. *J. Chem. Phys.* **1970**, *52*, 1058), close to where "anomalous" temperature behavior sets in.
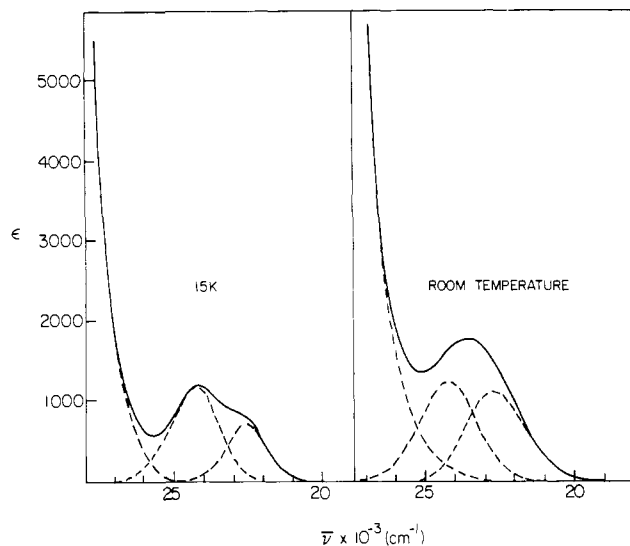
(46) Meyer, H. J. G. *Physica* **1955**, *21*, 253.

(47) The lower frequency of ν(Rh₂) for this complex accounts for both the extremely dramatic temperature dependence and the narrower bandwidths; that is, ν(Rh₂) is a lower-frequency, hence higher-amplitude mode, so Franck–Condon factors are smaller[39] for a given excited state ΔQ.

(48) Geoffroy, G. L.; Wrighton, M. S.; Hammond, G. S.; Gray, H. B. *Inorg. Chem.* **1974**, *13*, 430.

(49) Balch, A. L.; Olmstead, M. M. *J. Am. Chem. Soc.* **1979**, *101*, 3128.

Properties of Metal–Metal Single Bonds

J. Am. Chem. Soc., Vol. 107, No. 26, 1985 7933

Figure 12. Gaussian analysis of the $d\pi \rightarrow d\sigma^*$ absorption of $Rh_2b_4Cl_2^{2+}$ in LiCl(aq). See text.

Table VII. Parameters for Bands A and B[a]

band	$\bar{\nu}_{max} \times 10^{-3}$ (cm^{-1})	half-width (cm^{-1})	ϵ(max)	$f \times 10^2$
A (300 K)	22.60	2320	1210	1.29
A (15 K)	22.60	1610	780	0.58
B (300 K)	24.20	2260	1290	1.34
B (15 K)	24.25	1940	1270	1.13

[a] Evaluated from a Gaussian analysis of the spectra shown in Figure 11.

is $\pi^* \rightarrow \sigma^*$, with x,y ($\perp$ metal–metal) polarization; $\pi \rightarrow \sigma^*$ is x,y allowed in D_4 symmetry.

There are two components of the "$d\pi$" $\rightarrow d\sigma^*$ band of $Rh_2b_4Cl_2^{2+}$ at low temperature: a distinct shoulder at 22 500 cm^{-1}, and a maximum at 24 250 cm^{-1} (Figure 5). The "$d\pi$" $\rightarrow d\sigma^*$ band of $Rh_2(TMB)_4Cl_2^{2+}$ in PMM similarly shows a 23 500-cm^{-1} shoulder on a 25 000-cm^{-1} maximum. The "$d\pi$" $\rightarrow d\sigma^*$ band profile of $Rh_2b_4Cl_2^{2+}$ was analyzed both at room and low temperature as the sum of two Gaussians plus the Gaussian tail of the $d\sigma \rightarrow d\sigma^*$ band (Figure 12). Derived parameters are summarized in Table VII. The lower-energy band, labeled A, loses more than half of its intensity, whereas the higher energy band, B, loses less than 20%. The half-widths of these bands are much less temperature sensitive than those of the $d\sigma \rightarrow d\sigma^*$ transition, consistent with the expectation of a smaller excited-state distortion along the metal–metal coordinate.

Polarized single-crystal spectra in the region of the $d\sigma \rightarrow d\sigma^*$ system were obtained for $[Rh_2(TMB)_4Cl_2](PF_6)_2$ at 18 K (Figure 13). The crystal face available was (010) of the orthorhombic (*Pbcm*) crystal[7] for which, in the oriented-gas approximation, a transition polarized parallel to the rhodium–rhodium axis (z) should have 83% of its intensity ‖c and 17% ‖a. (A transition polarized $\perp z$ should have the inverse polarization ratio.) Thus the predominant ‖c polarization of the background confirms that most of the intensity is attributable to the higher-energy $d\sigma \rightarrow d\sigma^*$ transition. The low-energy shoulder (A of Figure 12) also is z polarized, but the other band (B of Figure 12) has mixed polarization.

(50) Evans, S.; Green, J. C.; Green, M. L. H.; Orchard, A. F.; Turner, D. W. *Discuss. Faraday Soc.* **1969**, *47*, 112.

(51) The criticism could be made that a long Rh–Rh bond length could result in very weak metal–metal coupling of π and δ symmetry orbitals, see: Hansen, A. E.; Ballhausen, C. J. *Trans. Faraday Soc.* **1965**, *61*, 631. Then the "$d\pi$" $\rightarrow d\sigma^*$ transitions should be assigned as $d_{xz}, d_{yz} \rightarrow d\sigma^*$, and $d_{xy} \rightarrow d\sigma^*$, where d_{xy}, etc., are essentially localized on single rhodium atoms. Predicted selection rules would be identical with those for $\pi^* \rightarrow d\sigma^*$ and $\delta^* \rightarrow d\sigma^*$. However, our viewpoint is that interactions with ligand π^* orbitals[35] will lead to strong coupling whether or not direct metal–metal coupling is significant.
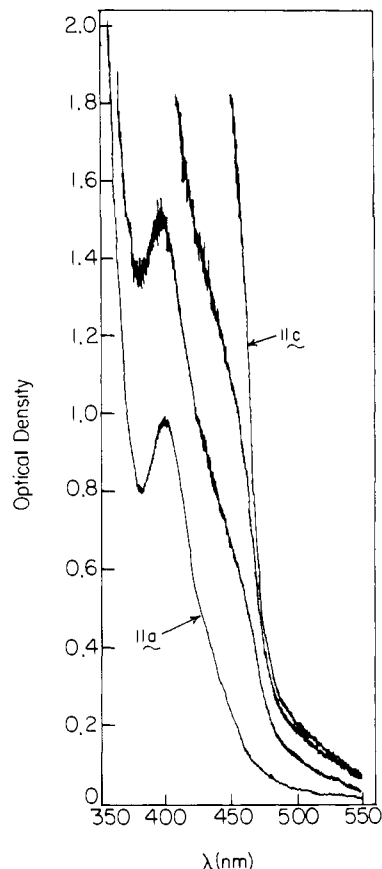
Figure 13. Polarized electronic spectra of the (010) face of a single crystal of $[Rh_2(TMB)_4Cl_2](PF_6)_2$ at 18 K: ‖a, ‖c, and two intermediate angles.
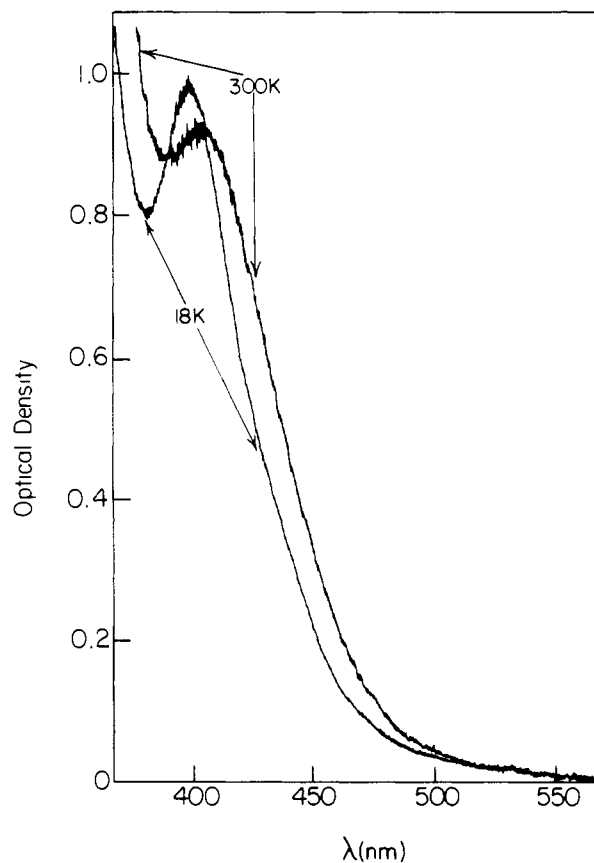
Figure 14. Polarized electronic spectra of the (010) face of a single crystal of $[Rh_2(TMB)_4Cl_2](PF_6)_2$: ‖a at 18 K and 300 K.

The ∥a spectra at room and low temperature are shown in Figure 14. The thermal behavior of band B in this polarization is that of an allowed transition; that is, the integrated intensity is temperature independent.

We conclude that band A is vibronically allowed ∥z, whereas B is dipole allowed ⊥z, but has considerable vibronically allowed ∥z intensity; thus, the isotropic intensity of B is less temperature sensitive than that of A. The obvious source of the vibronic intensity is the nearby z-allowed dσ → dσ* transition. On the basis of these results, band A is assigned to δ* → dσ* and band B to the x,y dipole-allowed dπ* → dσ*. The inferred δ*/π* splitting of ~1500 cm⁻¹ can be compared to the calculated[17a] and measured[16] splitting of ~2000 cm⁻¹ for $Rh_2(O_2CCH_3)_4(OH_2)_2$.

The "dπ" → dσ* band is less sensitive to axial ligands than dσ → dσ* (Tables V and VI). For the last entry of Table V, it seems to pass underneath dσ → dσ*. This trend is consistent with a model (Figure 6) in which most of the axial interaction involves the dσ (rather than the dσ*) orbitals.

Finally, we consider the weak bands to higher energy of dσ → dσ* (labeled III and IV in Table V). Figure 4 shows that both bands lose intensity at lower temperature, but our experience with band I indicates that this cannot disprove possible x,y-allowed character. Both III and IV are only weakly axial-ligand sensitive, and we therefore exclude LMCT assignments. Possible assignments are to the dπ → dσ* and dδ → dσ* transitions or to excitation from the various filled d-derived levels into the empty dσ*(Rh–C) orbitals. The energies of the latter transitions may be estimated by comparison to $Rh(CN)_6^{3-}$, which has its lowest singlet–singlet ligand-field transition at 230 nm (43 000 cm⁻¹).[48] We therefore suggest a ligand-field assignment for band IV. Band III is markedly asymmetric to higher energy in the low-temperature spectrum (Figure 5). Thus it may include both dδ → dσ* and dπ → dσ* excitations. The inferred total "dπ" splitting is ~10 000 cm⁻¹.

Photochemistry

We have obtained flash photolysis data for solutions of $Rh_2b_4Cl_2^{2+}$ on nanosecond[52] and picosecond[53] time scales. A small dσ → dσ* bleaching signal was observed, with a rise time of less than 20 ps. This signal, which remained invariant for greater than 100 ns, probably reflects reaction 4.

$$Rh_2b_4X_2^{2+} \xrightarrow{h\nu} Rh_2b_4X^{2+} + X\cdot \qquad (4)$$
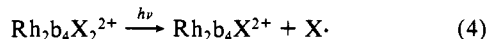
In support of this interpretation, we observed photoreduction (366-nm irradiation) of $Rh_2(TMB)_4Cl_2^{2+}$ and $Rh_2(TMB)_4Br_2^{2+}$ to $Rh_2(TMB)_4^{2+}$ in CH_3CN containing 1 M isopropyl alcohol,

with quantum yields of a few percent. Evidence for the halogen photoproduct Br_3^- was obtained from Raman experiments, as noted earlier. We also observed production of $Ir_2(TMB)_4^{2+}$ upon 254-nm irradiation of $Ir_2(TMB)_4Cl_2^{2+}$.

Evidently, the excited states of $Rh_2b_4Cl_2^{2+}$ have lifetimes of less than 20 ps, like those of $Mn_2(CO)_{10}$.[54] The characteristic deactivation pathway of the excited states of singly metal–metal bonded binuclear complexes, metal–metal bond scission,[54,55] is not an option for the bridged Rh^{II} and Ir^{II} complexes. The small amount of photoreduction observed is consistent with a moderate amount of axial ligand-to-metal charge-transfer character mixed into the dσ → dσ* state, as also inferred from our analysis of the electronic spectra. However, the dominant decay pathways seem to be very rapid nonradiative decay back to the ground state. We suggest that this may occur via a very-low-energy triplet dσ → dσ* state, which is metal–metal dissociative but can lead to no net reaction for the bridged complexes.

Concluding Remarks

While the work reported in this paper shows that the electronic spectra of dσ-bonded metal dimers can be rationalized in great detail, it appears that there is no simple correlation of dσ → dσ* band positions with ground-state bond distances and force constants. In a few favorable cases we do see a correlation: e.g., considerably larger metal–metal force constants for the Ir^{II} dimers correlate to considerably higher energy dσ → dσ* transitions, while a metal–metal bond ~0.4 Å shorter for[16] $Rh_2(O_2CCH_3)_4Cl_2^{2-}$ than for the isocyanide-ligated Rh^{II} dimers of this study does correlate with a ~13 000 cm⁻¹ higher energy dσ → dσ* transition.[16] However, the energy of the dσ → dσ* transition is perturbed greatly by LMCT mixing when the axial ligand is relatively reducing. In such cases the transition energies do not appear to be related simply to metal–metal force constants.

(52) Nanosecond laser flash photolysis experiments were done at the University of Southern California. The instrument has been described: Gutierrez, A. R.; Adamson, A. W. *J. Phys. Chem.* **1978,** *82,* 902.

(53) Picosecond laser flash photolysis experiments were performed by Prof. G. W. Scott at the University of California, Riverside. The 3rd harmonic (355 nm) of a Nd^{3+} glass laser was employed.

(54) (a) Freedman, A.; Bersohn, R. *J. Am. Chem. Soc.* **1978,** *100,* 4116. (b) Rothberg, L. J.; Cooper, N. J.; Peters, K. S.; Vaida, V. *J. Am. Chem. Soc.* **1982,** *104,* 3536.

(55) (a) Wrighton, M. S.; Ginley, D. S. *J. Am. Chem. Soc.* **1975,** *97,* 2065. (b) Hughey, J. L.; Anderson, C. P.; Meyer, T. J. *J. Organomet. Chem.* **1977,** *125,* C49.